Nonlinear pulse distortion in single-mode optical fibers at the zero-dispersion wavelength

Govind P. Agrawal
AT&T Bell Laboratories, 600 Mountain Avenue, Murray Hill, New Jersey 07974

M. J. Potasek
AT&T Engineering Research Center, P.O. Box 900, Princeton, New Jersey 08540
(Received 18 October 1985)

The propagation of optical pulses is considered at the zero-dispersion wavelength of nonlinear dispersive fibers. Even in the absence of group-velocity (first-order) dispersion, higher-order dispersive effects in single-mode silica fibers are found to be strong enough to cause significant broadening and distortion of picosecond optical pulses for fiber lengths of 10—100 km. Using the parameters appropriate for a 1.55-μm dispersion-shifted single-mode fiber, we have studied the evolution of pulse shapes and pulse spectra along the fiber length for a wide range of initial pulse widths. For peak powers $\sim$10 mW, the dispersive and nonlinear effects are comparable for pulse widths $\sim$1 ps and their mutual interplay leads to new qualitative features in the pulse shape and spectrum that are largely independent of the input profile. The theoretical results are useful for an understanding of the higher-order dispersion and, at the same time, have implications for high-capacity, long-haul, optical communication systems.

I. INTRODUCTION

Propagation of short, intense optical pulses through single-mode fibers is of considerable importance[1-9] because of the current interest in high-capacity, long-haul, optical communication systems. As pulses get shorter and more intense, both dispersive and nonlinear effects become increasingly more important. Under certain conditions a balance between the two effects can lead to soliton-like behavior[1,10,11] wherein the pulse propagates undistorted over long distances. In practice, more often than not, the group-velocity dispersion leads to considerable pulse broadening.[3,7] Commonly, one has attempted to avoid this dispersive broadening by operating the optical communication system at the so-called zero-dispersion wavelength (ZDWL) at which the fiber has the same group velocity for all frequencies associated with the pulse. For silica fibers, the ZDWL generally occurs in the vicinity of 1.3 μm.[12,13] It can be shifted to 1.55 μm by suitable design modifications in order to take advantage of the minimum fiber loss occurring at that wavelength. Such fibers are referred to as dispersion-shifted fibers and have attracted considerable attention recently.[14-17]

The chromatic dispersion, however, does not vanish entirely at the ZDWL, and higher-order dispersive effects should be considered for an appropriate modeling of the propagation characteristics of single-mode fibers.[5,6,9] Even when the nonlinear effects are negligible, higher-order dispersion can distort and broaden the optical pulses.[18,19] However, under typical operating conditions significant pulse distortion and broadening do not occur unless ultrashort ($\ll$1 ps) pulses are used. The situation can change dramatically when the nonlinear effects become important and need to be considered together with the higher-order dispersion. It is only recently that this case has attracted some attention.[5,6,9]

The object of this paper is to investigate in detail the propagation characteristics of short, intense optical pulses at the ZDWL of the single-mode fiber. By examining the relative contributions of the nonlinear and dispersive terms in the wave equation, we introduce the concept of a characteristic width τ_c such that the nonlinearity dominates when the initial pulse width $\tau_p \gg \tau_c$, while dispersion dominates when $\tau_p \ll \tau_c$. When the two are comparable, an interplay between the dispersive and nonlinear effects can give rise to new features. We consider pulse shapes and pulse spectra over a wide range of initial pulse widths and identify the role of nonlinearity. In particular, we find, in agreement with previous work,[5,6] that under certain conditions the nonlinearity can induce significant pulse broadening for fiber lengths in the range 10—100 km while almost none occurs in a linear medium.

For pulse widths $\tau_p \sim \tau_c$, the evolution of the pulse shape along the fiber length exhibits remarkably new qualitative features. The pulse consists of a number of subpulses whose width is determined by the higher-order dispersion alone at a given distance. Their relative amplitude is, however, governed by the nonlinearity and varies with the fiber length. In particular, the pulse shape exhibits a superstructure related to the nonlinearity-induced self-phase modulation. Similarly, the pulse spectrum consists of two parts: a central multipeak part arising from self-phase modulation and two narrow dominant peaks arising from the dispersion-induced subpulses in the pulse shape. Further, in the presence of fiber loss, after propagating a certain distance (about 50 km for 0.2 dB/km loss), the pulse acquires a spectrum that does not change with further propagation.

The paper is organized in the following way. In Sec. II we obtain the pulse-envelope equation starting from Maxwell's wave equation with particular attention paid to the assumptions and approximations made during its

derivation. We then describe the numerical procedure used to solve this equation that makes use of the Fourier-transform-based beam-propagation method.[20–24] By comparing the relative magnitudes of the dispersive and nonlinear effects, we introduce a characteristic time scale τ_c that is used to identify three distinct propagation regimes depending on the initial pulse width τ_p. Section III considers the nonlinearity-dominant regime $\tau_p \gg \tau_c$ where the qualitative features are governed mainly by the self-phase modulation. The dispersion-dominant regime $\tau_p \ll \tau_c$ is considered in Sec. IV. Here the pulse shapes are well described by the Airy function (linear-theory solution).[18] Using the stationary-phase method we show that the qualitative features in the dispersive regime are independent of the initial pulse shape. In Sec. V we consider the intermediate region where $\tau_p \sim \tau_c$ and the dispersive and nonlinear effects are comparable. Following the evolution of pulse shapes and spectra along the fiber length, we identify a number of new qualitative features. A simple model is used to obtain an approximate analytic solution that can explain reasonably well the numerically predicted results. Finally, the results are summarized in Sec. VI where we also discuss the feasibility of the experimental verification of the theoretical results.

II. WAVE EQUATION AND ITS NUMERICAL SOLUTION

A. Envelope equation

The starting point of our analysis is Maxwell's wave equation

$$\nabla^2 \mathbf{E} - \mu_0 \frac{\partial^2 \mathbf{D}}{\partial t^2} = 0 , \tag{2.1}$$

where $\mathbf{E}$ is the electric field, $\mathbf{D}$ is the electric displacement, and μ_0 is the vacuum permeability. The constitutive relation between $\mathbf{D}$ and $\mathbf{E}$ takes into account the dispersive and nonlinear nature of the fiber medium. If we assume that the medium responds instantaneously to the electric field, a suitable form for the constitutive relation is

$$\mathbf{D} \approx \epsilon_0 [n^2(\omega) + 2 n_0 n_2 |\mathbf{E}|^2] \mathbf{E} , \tag{2.2}$$

where ϵ_0 is the vacuum permittivity, $n_0 = n(\omega_0)$ is the linear index of refraction at the carrier frequency ω_0, and n_2 governs the strength of the nonlinear contribution to the dielectric constant. Using Eqs. (2.1) and (2.2), the wave equation becomes

$$\nabla^2 \mathbf{E} - \frac{1}{c^2} \frac{\partial^2}{\partial t^2} [n^2(\omega) \mathbf{E}] = \frac{2 n_0 n_2}{c^2} \frac{\partial^2}{\partial t^2} (|\mathbf{E}|^2 \mathbf{E}) , \tag{2.3}$$

where $c = (\mu_0 \epsilon_0)^{-1/2}$ is the speed of light in vacuum. In obtaining Eq. (2.3) we have assumed that the fiber medium is nonmagnetic and isotropic. The second term in Eq. (2.3) is to be interpreted in the time domain using the Fourier-transform correspondence $\omega \to i \partial / \partial t$, i.e.,

$$\frac{1}{c^2} \frac{\partial^2}{\partial t^2} [n^2(\omega) \mathbf{E}] = - \left[\beta \left(i \frac{\partial}{\partial t} \right) \right]^2 \mathbf{E} , \tag{2.4}$$

where

$$\beta(\omega) = \omega n(\omega) / c \tag{2.5}$$

is the propagation constant.

We consider wave propagation in a polarization-conserved single-mode fiber and write the electric field in the form

$$\mathbf{E}(\mathbf{r},t) = \hat{\mathbf{e}} U(\rho) A(z,t) \exp[-i(\omega_0 t - \beta_0 z)] , \tag{2.6}$$

where $\hat{\mathbf{e}}$ is the polarization unit vector, $U(\rho)$ is the field distribution in the radial direction ρ of the single mode supported by the fiber, $\beta_0 = n_0 \omega_0 / c$ is the propagation constant at the carrier frequency ω_0, and $A(z,t)$ is the (complex) amplitude of the pulse envelope. In the slow-varying-envelope approximation,

$$|\partial A / \partial z| \ll \beta_0 |A| \quad \text{and} \quad |\partial A / \partial t| \ll \omega_0 |A| . \tag{2.7}$$

We substitute Eq. (2.6) in Eq. (2.3), multiply by $U^*(\rho)$, and integrate over the transverse dimensions. Since the pulse spectrum is centered around ω_0, we expand $\beta(\omega)$ in a Taylor series about ω_0 and retain terms up to third order in $\omega - \omega_0$:

$$\beta(\omega) \approx \beta_0 + \beta^{(1)}(\omega - \omega_0) + \tfrac{1}{2} \beta^{(2)} (\omega - \omega_0)^2 + \tfrac{1}{6} \beta^{(3)} (\omega - \omega_0)^3 . \tag{2.8}$$

Here the derivatives $\beta^{(n)} = d^n \beta / d\omega^n$ are evaluated at the carrier frequency ω_0. It is convenient to introduce the reduced time (measured from the pulse center)

$$\tau = t - \beta^{(1)} z . \tag{2.9}$$

Using Eqs. (2.7)–(2.9), the pulse-envelope amplitude is found to satisfy the following equation:

$$i \frac{\partial A}{\partial z} + i \gamma A - \frac{1}{2} \beta^{(2)} \frac{\partial^2 A}{\partial \tau^2} - \frac{i}{6} \beta^{(3)} \frac{\partial^3 A}{\partial \tau^3} + \frac{\bar{n}_2 \omega_0}{c} |A|^2 A + \frac{2 i \bar{n}_2}{c} \frac{\partial}{\partial \tau} (|A|^2 A) = 0 , \tag{2.10}$$

where we have added a loss term with the amplitude-absorption coefficient γ to account for the fiber loss. In Eq. (2.10), $\bar{n}_2$ is the effective nonlinear coefficient

$$\bar{n}_2 = \left(\int_{-\infty}^{\infty} |U(\rho)|^4 \rho \, d\rho \Big/ \int_{-\infty}^{\infty} |U(\rho)|^2 \rho \, d\rho \right) n_2 \tag{2.11}$$

modified to account for the transverse variation of the fiber mode.

Equation (2.10) describes the propagation of an optical pulse in a dispersive nonlinear medium. The coefficients $\beta^{(2)}$ and $\beta^{(3)}$ take into account chromatic dispersion and are sometimes referred to as the first- and second-order dispersion coefficients. Generally, $\beta^{(2)}$ dominates and the contribution of $\beta^{(3)}$ can be neglected. At the ZDWL, $\beta^{(2)} = 0$ and $\beta^{(3)}$ has to be included. The last term in Eq. (2.10) is responsible for self-steepening and can be neglected in most cases of practical interest when the pulse is neither too short nor too intense (pulse width $\gtrsim 0.1$ ps and the peak power $\lesssim 1$ W). The pulse propagation at the ZDWL of the fiber is then governed by

$$\frac{\partial A}{\partial z}=-\gamma A+\frac{1}{6}\beta^{(3)}\frac{\partial^3 A}{\partial \tau^3}+\frac{i\bar{n}_2\omega_0}{c}|A|^2A \ . \quad (2.12)$$

This is a nonlinear, third-order, partial differential equation whose analytic solution is generally not available, making it necessary to employ numerical techniques.

B. Numerical procedure

We solve Eq. (2.12) numerically using the Fourier-transform-based beam-propagation technique.[20–24] Equation (2.12) is written formally as

$$\frac{\partial A}{\partial z}=(D+N)A \ , \quad (2.13a)$$

where the differential operator D includes the first two terms involving loss and dispersion while N consists of the last nonlinear term, i.e.,

$$D\left[\frac{\partial}{\partial \tau}\right]=-\gamma+\frac{1}{6}\beta^{(3)}\frac{\partial^3}{\partial \tau^3}, \quad N(A)=\frac{i\bar{n}_2\omega_0}{c}|A|^2 \ . \quad (2.13b)$$

An exact solution of Eq. (2.13) is difficult to obtain because of the noncommutating nature of the operators D and N. However, an approximate solution can be obtained using the following split-step procedure[21–24] to propagate the complex field $A(z,\tau)$ by a small distance δ:

$$A(z+\delta,\tau)=\left[e^{\delta D/2}\exp\left[\int_z^{z+\delta}N(z')dz'\right]e^{\delta D/2}\right]A(z,\tau) \ . \quad (2.14)$$

The numerical procedure consists of propagating the field for a distance $\delta/2$ with dispersion only, multiplying the result by a nonlinear term that represents the effect of nonlinearity over the whole segment length δ, and then propagating the field for the remaining distance $\delta/2$ with dispersion only. In effect, the nonlinearity is assumed to be lumped at the midplane of each segment. The beam-propagation technique has been widely used in analyzing unstable resonators,[20] atmospheric propagation,[23] semiconductor lasers,[24] and pulse propagation in fibers.[3,21]

The propagation in a linear dispersive medium governed by the exponential operator $\exp(\delta D/2)$ in Eq. (2.14) can be accomplished using the Fourier-transform method, i.e.,

$$A(z+\delta/2,\tau)=\exp(\delta D/2)A(z,\tau)=\left[F^{-1}\exp\left[\frac{\delta}{2}D(i\omega)\right]F\right]A(z,\tau) \ , \quad (2.15)$$

where F denotes the Fourier-transform operation, $D(i\omega)$ is obtained using Eq. (2.13b), and ω is the frequency in the Fourier space. The use of the fast-Fourier-transform algorithm[25] makes numerical evaluation of Eq. (2.15) relatively fast. Equation (2.14) can then be used repeatedly to propagate the optical pulse through a given length of fiber after suitably choosing the step size δ.

Care must be exercised in evaluating the integral appearing in Eq. (2.14). If we use the trapezoidal rule, the integral can be approximated by

$$\int_z^{z+\delta}N(z')dz'=[N(z)+N(z+\delta)]\frac{\delta}{2} \ , \quad (2.16)$$

where $N=i\bar{n}_2(\omega_0/c)|A|^2$. However, $N(z+\delta)$ cannot be evaluated since $A(z+\delta,\tau)$ is not known while evaluating Eq. (2.16) at the midsegment located at $z+\delta/2$. We have followed an iterative procedure that is initiated by replacing $N(z+\delta)$ with $N(z)$ in Eq. (2.16). Equation (2.14) is then used to estimate $A(z+\delta,\tau)$ which in turn is used to calculate the new value of $N(z+\delta)$. We have found that two iterations are enough in practice. The iterative procedure can, of course, be avoided by decreasing δ until the desired accuracy is achieved This may, however, increase the computing time substantially.

C. Three propagation regimes

Numerical solutions of Eq. (2.12) under various initial conditions show that depending on the initial pulse width τ_p, three different regimes with different propagation characteristics exist. These three regimes can be characterized in terms of a characteristic time τ_c defined such that when the pulse width $\tau_p\sim\tau_c$, the dispersive and nonlinear contributions are comparable. To obtain a quantitative estimate of τ_c, we consider the ratio of the nonlinear to the dispersive terms in Eq. (2.12) and obtain

$$R=\left|\frac{N}{D}\right|=\frac{6\bar{n}_2\omega_0|A|^2}{c\beta^{(3)}}\left|\frac{1}{A}\frac{\partial^3 A}{\partial \tau^3}\right|^{-1} \ . \quad (2.17)$$

Clearly, the ratio R varies with z and τ. We evaluate it at the initial plane $z=0$ and assume that a Gaussian pulse with amplitude

$$A(0,\tau)=A_0\exp(-\tau^2/2\tau_p^2) \quad (2.18)$$

is launched into the fiber. Here A_0 is the peak amplitude and τ_p is the half-width at which the intensity drops by $1/e$. Using Eqs. (2.17) and (2.18), we obtain

$$R=\frac{6\bar{n}_2\omega_0A_0^2\tau_p^3}{c\beta^{(3)}}\left|\frac{\exp(-x^2)}{x(3-x^2)}\right| \ , \quad (2.19)$$

where $x=\tau/\tau_p$.

We define the characteristic time τ_c as the pulse width τ_p for which $R_{\max}=1$. The maximum value of R occurs for $x=1.478$ in Eq. (2.19). Using this value of x and setting $R_{\max}=1$, we obtain

$$\tau_c=\left[\frac{1.8c\beta^{(3)}}{\bar{n}_2A_0^2\omega_0}\right]^{1/3} \ . \quad (2.20)$$

The three propagation regimes are thus identified as follows: (i) When $\tau_p\gg\tau_c$, nonlinearity dominates over dispersion; (ii) when $\tau_p\ll\tau_c$, dispersion dominates over nonlinearity; and (iii) when $\tau_p\sim\tau_c$, the two are equally important. We use τ_p as a measure of pulse width for simplicity. The corresponding full width at half maximum for a Gaussian pulse is obtained by multiplying it by the numerical factor of $2\sqrt{\ln 2}\simeq 1.66$.

In the following three sections we consider each regime separately. For our numerical calculations, we consider the realistic case of dispersion-shifted fibers with the ZDWL at 1.55 μm.[16] In particular, we consider a

triangular-core fiber with the core diameter of 6.5 μm and the relative core-cladding index difference $\Delta=0.01$. These are typical values for such fibers. The value of the second-order dispersion coefficient, estimated from the measured dispersion data, is $\beta^{(3)}=0.2$ ps^3/km. The measured value of $n_2=1.14\times10^{-13}$ esu for silica fibers.[26] To obtain $\bar{n}_2$, the integrals in Eq. (2.11) are performed with the Gaussian approximation for the fundamental fiber mode, and we obtain $\bar{n}_2=n_2/2$. For the fiber parameters considered here the effective Gaussian-mode cross section is estimated to be 7.6 μm^2. The nonlinear contribution is directly proportional to the input peak power P_0. For a power level $P_0=20$ mW, $\bar{n}_2A_0^2\simeq1.67\times10^{-10}$. Using these parameter values in Eq. (2.20), we obtain $\tau_c\simeq0.8$ ps. In all calculations the fiber loss is fixed at 0.2 dB/km which corresponds to $\gamma=0.023$ km^{-1} in Eq. (2.12). The peak power of the input pulse is chosen to be 20 mW. The nonlinear parameter $\bar{n}_2(\omega_0/c)A_0^2=0.68$ km^{-1}, corresponding to this power level. It should be noted that for a given peak power, the nonlinear parameter depends on the fiber-mode cross section which in turn depends on the core diameter and the core-cladding index difference.

In the following numerical results, Eq. (2.12) is solved using Eqs. (2.14)–(2.16) with the initial Gaussian profile (2.18) at the plane $z=0$. After propagating a certain distance, the calculated amplitude $A(z,\tau)$ is used to obtain the temporal intensity profile (pulse shape) $|A(z,\tau)|^2$ and the spectral profile $G(z,\omega)$. The latter is calculated using

$$G(z,\omega)=\left|\int_{-\infty}^{\infty}A(z,\tau)\exp[-i(\omega-\omega_0)]d\tau\right|^2. \quad (2.21)$$

The nonlinear and dispersive effects manifest through the changes in both the pulse shape and the pulse spectrum. We now present the temporal and spectral profiles for a wide range of input pulse widths. For the sake of comparison, the temporal profiles are normalized such that $A(0,0)=1$ and are shown after excluding the intensity reduction $\exp(-2\gamma z)$ due to linear absorption so that the pulse area remains constant during propagation. The spectral profiles are normalized to unit maximum amplitude and are centered at the carrier frequency ω_0.

III. DOMINANT NONLINEARITY

This section considers the case of relatively broad pulses compared to the characteristic width τ_c. Figure 1 shows the intensity and spectral profiles at $z=50$ km for $\tau_p=25$ ps. Dashed curves show, for comparison, the corresponding initial profiles at $z=0$. We notice that the pulse shape has hardly changed whereas the pulse spectrum has broadened considerably with an oscillatory structure. This spectral broadening is a consequence of self-phase modulation induced by the nonlinearity and has been previously studied.[26–29] The effect of second-order dispersion is to introduce an asymmetry, seen clearly in the pulse spectrum of Fig. 1. This is, however, a minor effect in the regime where the nonlinearity is dominant.

A qualitative understanding of the propagation characteristics in the nonlinearity-dominant regime can be developed by neglecting the dispersion altogether and setting $\beta^{(3)}=0$ in Eq. (2.12). The resulting differential equation can be solved analytically with the result

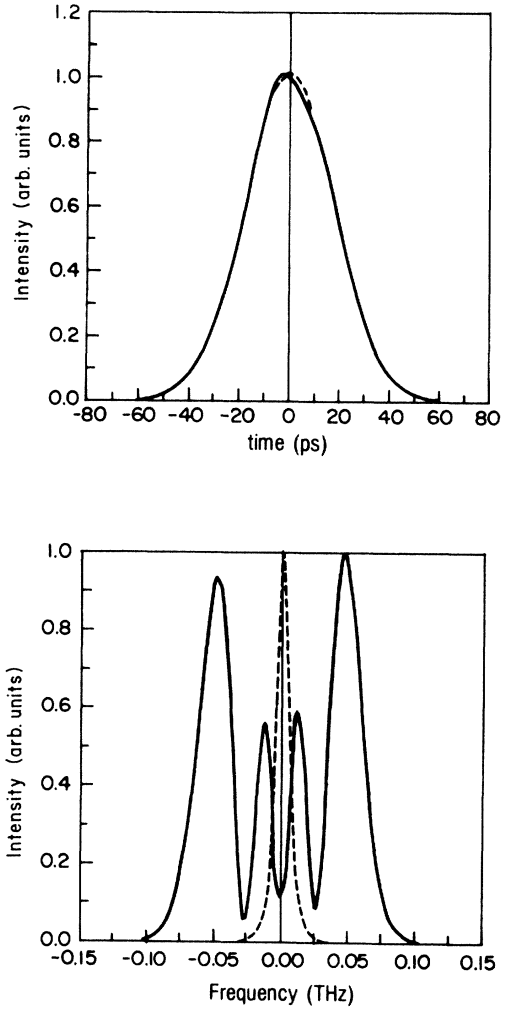

FIG. 1. Temporal and spectral profiles at $z=50$ km for a Gaussian pulse with $\tau_p=25$ ps. Dashed curves show the corresponding initial profiles at $z=0$. Here and in all subsequent figures $\gamma=0.2$ dB/km, $\beta^{(3)}=0.2$ ps^3/km, and input peak power $A_0^2=20$ mW.

$$A(z,\tau)=A(0,\tau)e^{-\gamma z}\times\exp\left[i\frac{\bar{n}_2\omega_0}{c}\left(\frac{1-e^{-2\gamma z}}{2\gamma}\right)|A(0,\tau)|^2\right]. \quad (3.1)$$

Since the nonlinearity affects only the phase of the propagating pulse, the pulse shape does not change during propagation except for an overall loss-induced amplitude reduction. However, the resulting self-phase modulation significantly affects the pulse spectrum. This can be seen by substituting Eq. (3.1) in Eq. (2.21). For a Gaussian pulse with the amplitude $A(0,\tau)$ given by Eq. (2.18), the spectrum is given by

$$G(z,\omega)=A_0^2e^{-2\gamma z}\left|\int_{-\infty}^{\infty}\exp(-\tau^2/2\tau_p^2)\times\exp(i\phi_m e^{-\tau^2/\tau_p^2})\times\exp[-i(\omega-\omega_0)\tau]d\tau\right|^2, \quad (3.2)$$

where

$$\phi_m = \frac{\bar{n}_2 \omega_0}{c} \left[\frac{1-e^{-2\gamma z}}{2\gamma} \right] A_0^2 \tag{3.3}$$

is the maximum phase shift due to self-phase modulation. By expanding the second exponential in Eq. (3.2), the integral can be performed to yield the series solution

$$G(z,\omega) = A_0^2 e^{-2\gamma z} \left| \sum_n \frac{(i\phi_m)^n}{n!} \left[\frac{2\pi\tau_p^2}{2n+1} \right]^{1/2} \times \exp\left[-\frac{(\omega-\omega_0)^2 \tau_p^2}{2(2n+1)} \right] \right|^2 . \tag{3.4}$$

The numerical evaluation of Eq. (3.2) or Eq. (3.4) shows that the spectrum for the purely nonlinear case ($\beta^{(3)}=0$) is similar to that shown in Fig. 1 but without the dispersion-induced asymmetry.

The qualitative features of the pulse spectrum can be understood through the time-dependent nonlinearity-induced phase shift

$$\phi_N = \phi_m \exp(-\tau^2/\tau_p^2) \tag{3.5}$$

occurring in Eq. (3.2). The effect of self-phase modulation is to chirp the pulse or induce a frequency shift $\delta\omega = \partial\phi_N/\partial t$. The oscillatory structure seen in Fig. 1 arises from an interference between the two spectral components for which the frequency shift is the same.[27] The extent of spectral broadening $\Delta\omega$ on each side of the optical frequency is given approximately by $|\partial\phi_N/\partial\tau|_{\max}$. One can readily verify that $\Delta\omega \sim \phi_m/\tau_p$. Since τ_p^{-1} is the spectral width in the absence of self-phase modulation, the spectrum is broadened by a factor of ϕ_m, where ϕ_m is given by Eq. (3.3). We note that the numerical value of ϕ_m is loss dependent. In the absence of loss ($\gamma=0$), ϕ_m increases linearly with z, and the spectrum would keep broadening with more and more peaks in Fig. 1. However, ϕ_m saturates for finite value of γ for distances $z \gtrsim \gamma^{-1}$. For the value $\gamma=0.2$ dB/km used in Fig. 1, the saturation has nearly occurred for $z=50$ km, and no further spectral changes occur with an increase in the fiber length. The number of peaks is given by the integer part of $2\phi_m/2\pi$, and four peaks occur since $\phi_m \approx 15$ for the parameter values used for Fig. 1.

IV. DOMINANT DISPERSION

In this section we consider the case of ultrashort pulses with width $\tau_p \ll \tau_c$. Figure 2 shows the intensity and spectral profiles for $\tau_p=50$ fs at the output end of a fiber of length $z=5$ m. In contrast to Fig. 1, the spectral profile is almost identical to the initial profile at $z=$ On the other hand, the pulse acquires significant structure on the trailing edge appearing in the form of subpulses of decreasing amplitudes as τ increases. (The dispension-induced subpulses appear on the leading edge when $\beta^{(3)}$ is negative.) Since the nonlinearity does not play a significant role in the dispersion-dominant regime, the qualitative behavior can be reasonably well understood by dropping the nonlinear term in Eq. (2.12). The resulting linear equation can be readily solved using the Fourier-transform technique with the solution

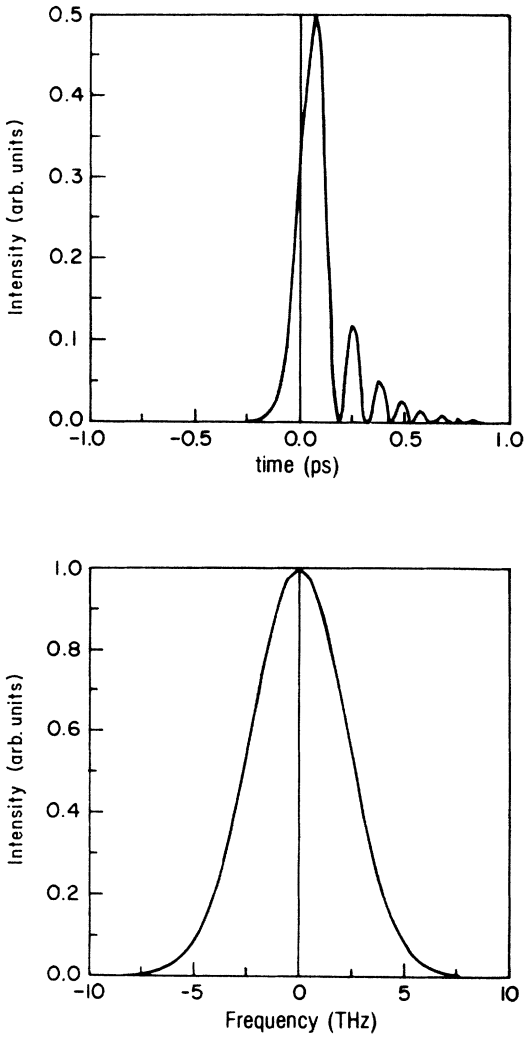

FIG. 2. Temporal and spectral profiles at $z=5$ m for a Gaussian pulse with $\tau_p=0.05$ ps. Other parameters are the same as in Fig. 1. For such narrow pulses, dispersion dominates over nonlinearity and generates additional subpulses on the leading edge of the pulse. The pulse spectrum is indistinguishable from the initial spectrum at $z=0$.

$$A(z,\tau) = e^{-\gamma z} \int_{-\infty}^{\infty} \tilde{A}(0,\omega) \exp\left[i\omega\tau - \frac{i}{6}\beta^{(3)}\omega^3 z \right] d\omega , \tag{4.1}$$

where

$$\tilde{A}(0,\omega) = \frac{1}{2\pi} \int_{-\infty}^{\infty} A(0,\tau) \exp(-i\omega\tau) d\tau \tag{4.2}$$

is the spectrum at $z=0$. For a Gaussian pulse with $A(0,\tau)$ given by Eq. (2.18), $\tilde{A}(0,\omega)$ is also Gaussian. The integration in Eq. (4.1) in this specific case leads to the analytic solution[18]

$$A(z,\tau)=\frac{2}{\sqrt{\pi}}e^{-\gamma z}(\bar{z})^{-1/3} \times\exp\left[\frac{2-3\bar{\tau}\bar{z}}{3\bar{z}^2}\right]\mathrm{Ai}[(1-\bar{\tau}\bar{z})\,|\,\bar{z}\,|^{-4/3}]\,, \tag{4.3}$$

where $\bar{\tau}$ and $\bar{z}$ are the normalized width and distance defined using

$$\bar{\tau}=\sqrt{2}\tau/\tau_p,\quad \bar{z}=\sqrt{2}\beta^{(3)}z/\tau_p^3\,, \tag{4.4}$$

and $\mathrm{Ai}(x)$ is the Airy function.[30]

The qualitative behavior seen in Fig. 2 can be understood using the Airy-function solution (4.3) obtained for the linear dispersive medium. The Airy function $\mathrm{Ai}(x)$ exhibits oscillations for negative values of its argument x. It is thus evident from Eq. (4.3) that the pulse amplitude would exhibit oscillations (or ringing) when $\bar{\tau}\bar{z}>1$, or using Eq. (4.4), when

$$\tau>\tau_d=\tau_p^4/(2\beta^{(3)}z)\,. \tag{4.5}$$

For small distances z such that $\tau_d\gg\tau_p$, the oscillations would not be apparent since their amplitude is very small. However, if $\tau_d\lesssim\tau_p$, the pulse would contain oscillatory structure for $\tau>\tau_d$. Using this criterion, one can estimate the distance above which the oscillatory structure becomes apparent. Setting $\tau_d=\tau_p$ in Eq. (4.5), this critical distance is given by

$$z_c=\tau_p^3/2\beta^{(3)}\,. \tag{4.6}$$

If we use $\tau_p=0.05$ ps and $\beta^{(3)}=0.2$ ps^3/km, the parameters used to obtain Fig. 2, we find that the distance z_c is about 0.3 m. As the distance increases, more and more subpulses are added to the trailing edge ($\tau>0$) of the pulse. One can estimate the number and width of these subpulses by using the following asymptotic expansion[30] of $\mathrm{Ai}(x)$, valid for large negative values of x:

$$\mathrm{Ai}(x)\simeq\frac{1}{\sqrt{\pi}}\,|\,x\,|^{-1/4}\sin(\tfrac{2}{3}\,|\,x\,|^{3/2}+\tfrac{1}{4}\pi)\,, \tag{4.7}$$

where on using Eqs. (4.3) and (4.4)

$$x\simeq-\bar{\tau}\bar{z}\,|\,\bar{z}\,|^{-4/3}=-(2\tau^3/\beta^{(3)}z)^{1/3}\,. \tag{4.8}$$

The pulse intensity becomes zero whenever the argument of the sine function in Eq. (4.7) is an integer multiple of 2π, i.e.,

$$\tfrac{2}{3}\,|\,x\,|^{3/2}+\tfrac{1}{4}\pi=2\pi m\,, \tag{4.9}$$

or after using Eq. (4.8),

$$\tau_m=\left[\frac{9\pi^2}{8}\beta^{(3)}z(2m-\tfrac{1}{4})^2\right]^{1/3}\quad(m>0)\,, \tag{4.10}$$

where τ_m is the value of τ for the mth zero. Equation (4.10) shows that the location of subpulses (zeros in the pulse intensity) varies with distance. Further, their widths at a given distance z are not the same and decrease slowly as m increases. Our numerical results verify these conclusions in the dispersion-dominant regime. The amplitude and the number of subpulses are determined by the exponential term in Eq. (4.3) which governs the overall envelope of the pulse structure. Using Eqs. (4.3) and (4.4), the envelope is given approximately by $\exp(-\tau/\tau_0)$, where $\tau_0=\beta^{(3)}z/\tau_p^2$. Thus the amplitude of the subpulses decays exponentially and only a few pulses with $\tau_m\lesssim\tau_0$ would have noticeable amplitude.

The previous discussion of the dispersion-induced subpulses is based on the Airy-function solution (4.3) obtained for an initially Gaussian pulse. The phenomenon is, however, expected to be general, and qualitatively similar results should hold for other pulse shapes. In the Appendix the integral (4.1) is evaluated asymptotically for arbitrary pulse shapes using the method of stationary phase. We find that the effect of pulse shape is to modify the envelope of the subpulses while their width, governed by Eq. (4.10), remains unaffected. This feature is illustrated in Fig. 3 where the pulse shape and spectrum are plotted for a pulse with secant-hyperbolic profile at $z=0$, i.e.,

$$A(0,\tau)=A_0\,\mathrm{sech}(\tau/\tau_p)\,. \tag{4.11}$$

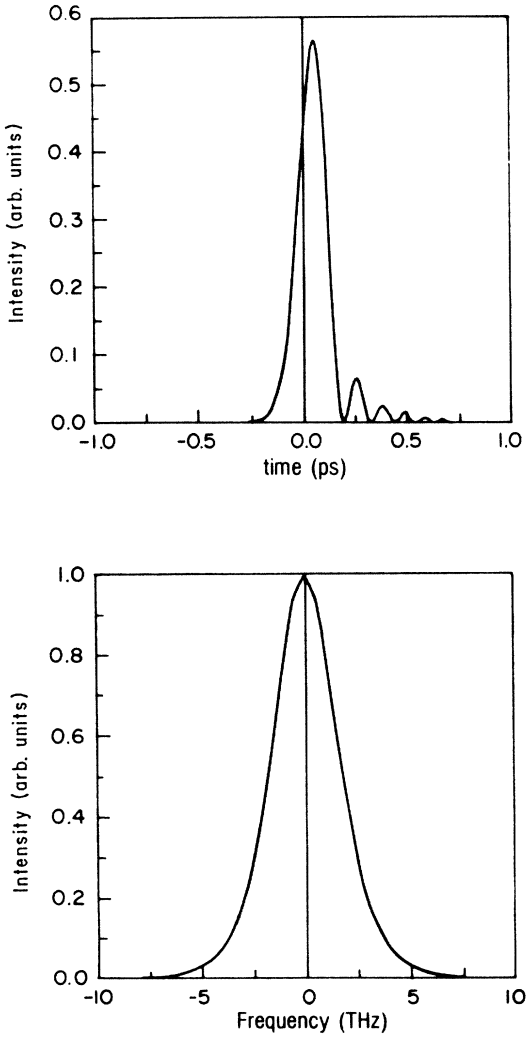

FIG. 3. Same as in Fig. 2 except that the pulse shape is governed by $\mathrm{sech}(\tau/\tau_p)$. Compare with Fig. 2 and note the similarity in pulse shapes except for the pulse heights. In particular, intensity minima occur at the same locations.

The other parameters are the same as in Fig. 2. A comparison of Figs. 2 and 3 shows that except for the height of the subpulses, the dispersion-induced features are independent of the initial pulse shape. In particular, the locations of the subpulses (intensity minima) are the same in the two cases.

V. DISPERSION AND NONLINEARITY COMPARABLE

The preceding results have shown that depending on whether the nonlinearity or the dispersion dominates, either the pulse spectrum or the pulse shape is mainly affected during propagation. In this section we consider the important intermediate region wherein the dispersion and the nonlinearity are comparable. As a result, their mutual interaction plays an important role, and new qualitative features arise.

Figure 4 shows the pulse shape and the spectrum for an input pulse with $\tau_p = 1$ ps at a distance $z = 5$ km. Since τ_p is comparable to the characteristic time $\tau_c = 0.8$ ps [see Eq. (2.20)], both the shape and spectrum are affected during propagation. In particular, the dispersive effects governed by $\beta^{(3)}$ introduce oscillatory structure (subpulses) in the pulse shape. However, in contrast to the result shown in Fig. 2, the modulation is not complete, i.e., the intensity minima do not go to zero. Similarly, the asymmetric double-peak spectrum is very different from the nonlinearity-dominant case shown in Fig. 1. As a result of interplay between the dispersion and the nonlinearity, none of the analytic results presented in Secs. III and IV are applicable here.

Further propagation of the optical pulse inside the fiber reveals additional new qualitative features. Figure 5 shows the pulse shape and the spectrum at $z = 25$ km and should be compared with Fig. 4. The pulse exhibits a large number of dispersion-generated subpulses. Howev-

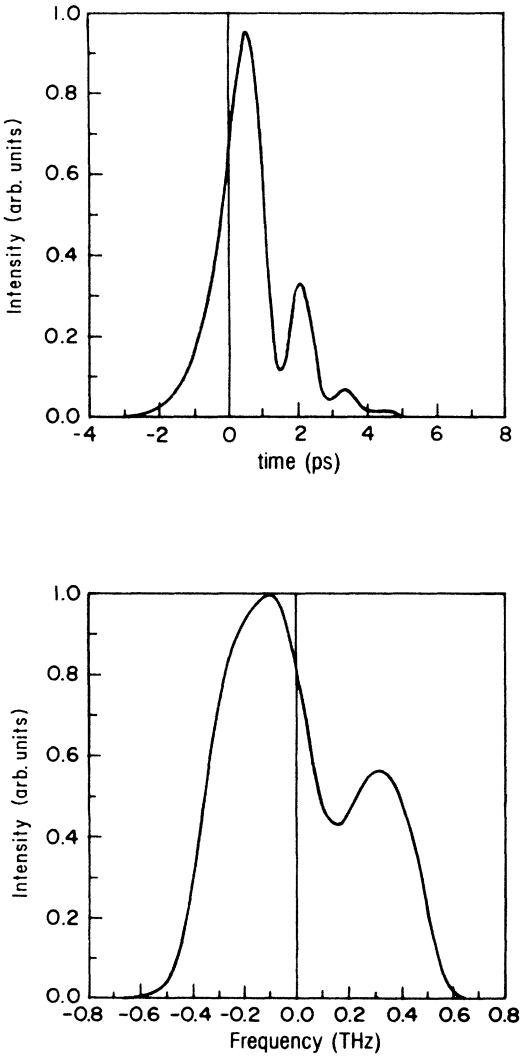

FIG. 4. Temporal and spectral profiles at $z = 5$ km for a Gaussian pulse with $\tau_p = 1$ ps. Note that in contrast to Figs. 1 and 2, both the shape and spectrum are affected by dispersion and nonlinearity.

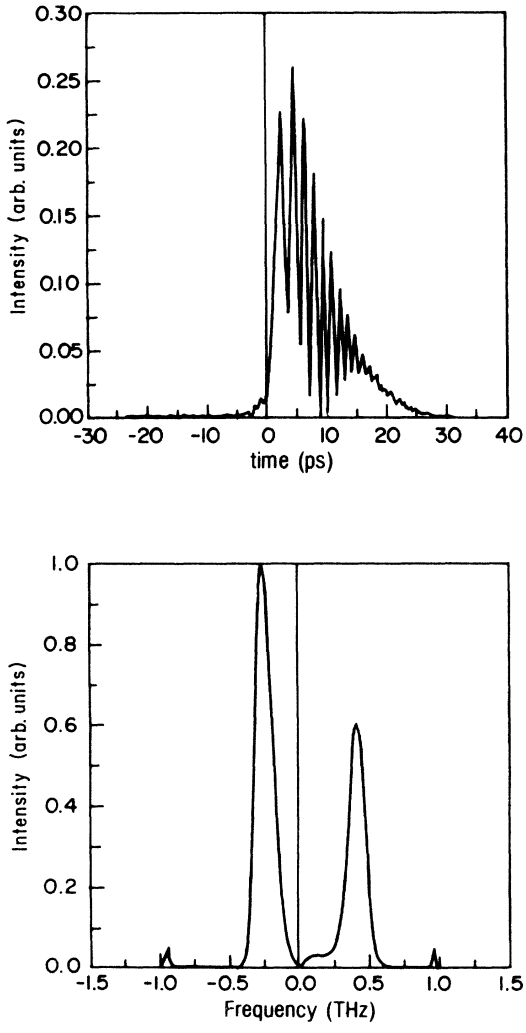

FIG. 5. Same as in Fig. 4 except that the 1-ps pulse has propagated to $z = 25$ km. Note the discrete nature of the pulse spectrum with peaks at multiples of a characteristic frequency ~ 400 GHz related to the repetition rate of the subpulses in the temporal profile.

er, a remarkable feature is that the first subpulse is no longer the most intense one (as expected for the purely dispersive case). Apparently, the nonlinearity is shifting the power distribution among various subpulses. The spectrum in Fig. 5 is dominated by two peaks occurring at about ± 400 GHz on both sides of the optical frequency. These peaks are a manifestation of the periodic structure of subpulses in the pulse shape and their frequency is approximately given by the repetition rate of subpulses. The additional side peaks at twice the fundamental frequency also occur since the subpulse structure is not exactly periodic.

In order to explore fully the propagation features, we have followed the evolution of an initial Gaussian pulse with $\tau_p = 2.5$ ps from $z = 0$ to 100 km. This corresponds to a full width at half maximum of about 4 ps. In Figs. 6 and 7 we show the pulse shapes and spectra at several values of z. Figure 8 shows the details of the pulse breakup during the early stages on an expanded scale. As before, dispersion generates subpulses whose number increases rapidly with z. As a result, there is a huge broadening on the trailing edge of the pulse. (For negative values of $\beta^{(3)}$, the pulse shapes are mirror images of those shown in Fig. 6 and the broadening is on the leading edge of the pulse.) The relative amplitude of various subpulses changes with z and appears to be governed by the nonlinear effects. In particular, the envelope develops a two-peak superstructure whose origin, as will be shown

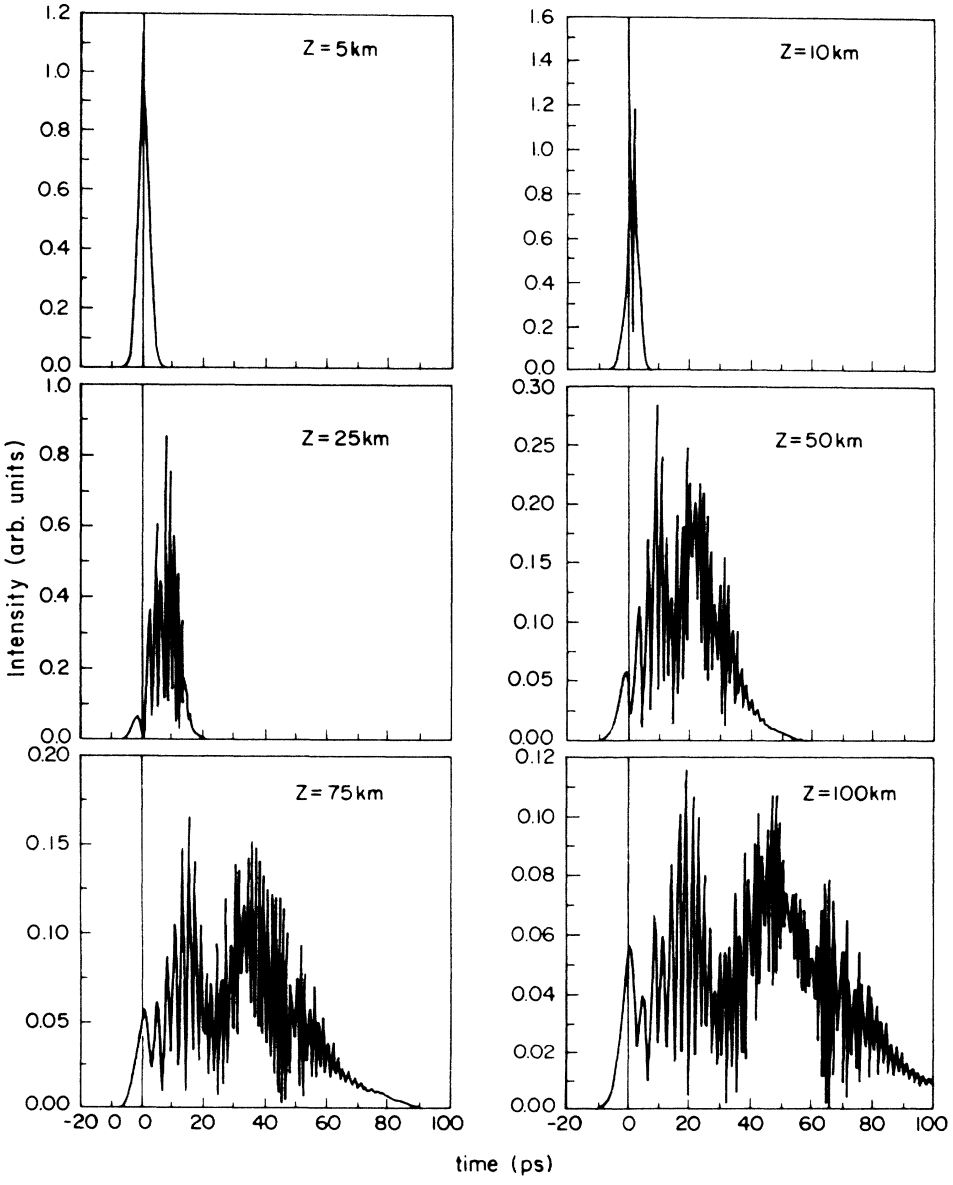

FIG. 6. Evolution of the pulse shape along the fiber length for a Gaussian pulse with $\tau_p = 2.5$ ps. The pulse broadens as a consequence of dispersion-generated subpulses and develops a two-peak superstructure that is related to the nonlinearity-induced self-phase modulation.

below, can be traced to the self-phase-modulation-induced spectral broadening.

The evolution of the pulse spectrum shown in Fig. 7 exhibits a number of interesting features. Although it appears to have a complicated shape, the spectrum consists of two parts. First, there occur two narrow peaks at about ± 400 GHz similar to the case shown in Fig. 5. These peaks are related to the almost periodic subpulse structure generated by the dispersion. Second, there are additional peaks of much lower amplitude in the central part of the spectrum. These peaks are related to the nonlinearity-induced self-phase modulation (see Fig. 1) and their number increases with the distance propagated inside the fiber. However, as already discussed in Sec. III, in the presence of loss their number eventually saturates after some distance $z \gtrsim \gamma^{-1}$. For the case of 0.2-dB/km loss considered here, the saturation occurs around 50 km. For this reason, no spectral changes are expected to occur with a further increase in z. This is clearly seen in Fig. 7 for $z = 50$, 75, and 100 km where the spectrum appears to be "frozen." The important point to note is that the spectrum is dominated by the dispersion-induced peaks rather than by the nonlinearity-induced central structure.

In order to understand physically the qualitative features of the pulse-evolution process, we obtain an approximate analytic solution of Eq. (2.12) using a simple model. Whereas the dispersive and nonlinear mechanisms act simultaneously to shape the optical pulse, the model

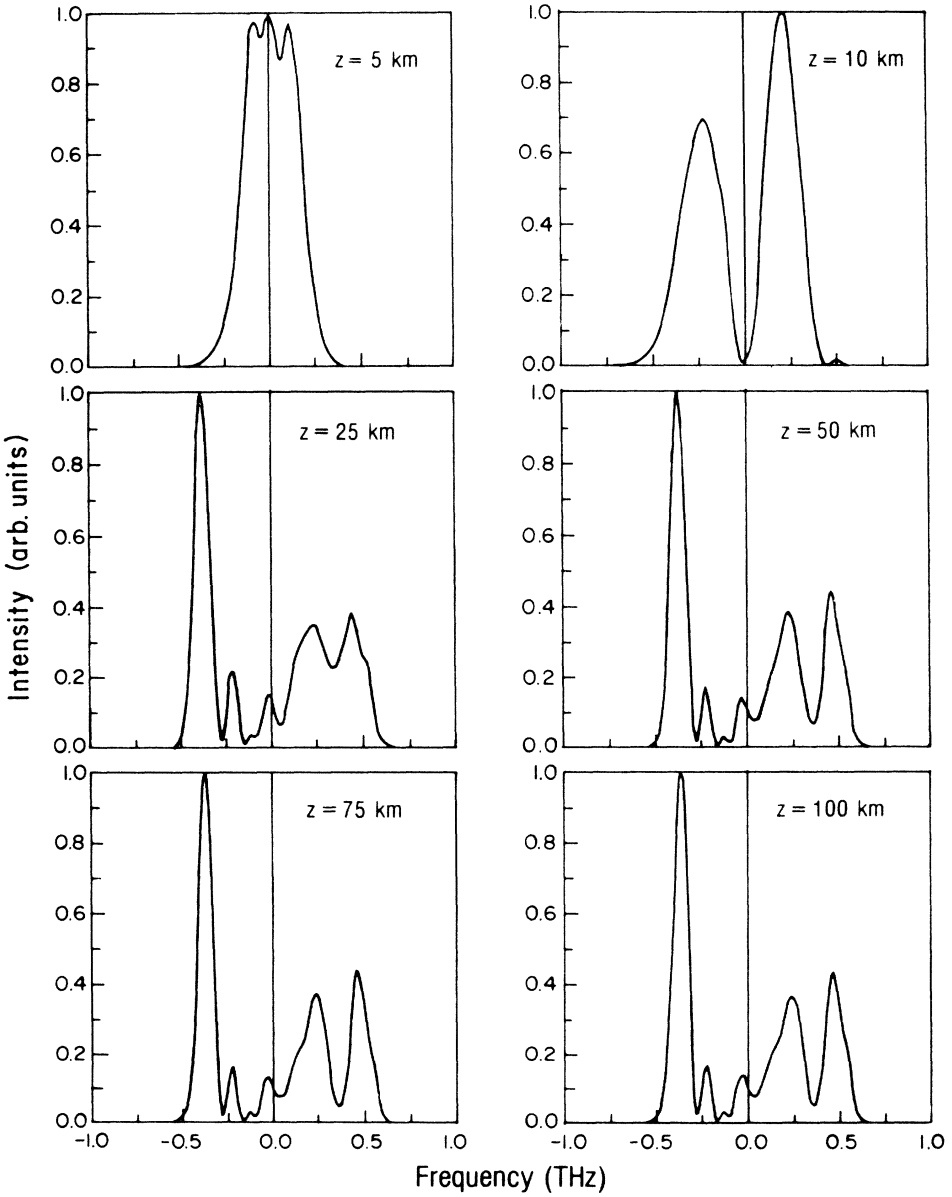

FIG. 7. Evolution of the pulse spectrum along the fiber length for a Gaussian pulse ($\tau_p = 2.5$ ps) whose temporal evolution is shown in Fig. 6. For $z > 50$ km, the spectrum does not change with propagation. The two extreme peaks are related to the subpulse structure (see Fig. 6) while the central part is related to the self-phase modulation.

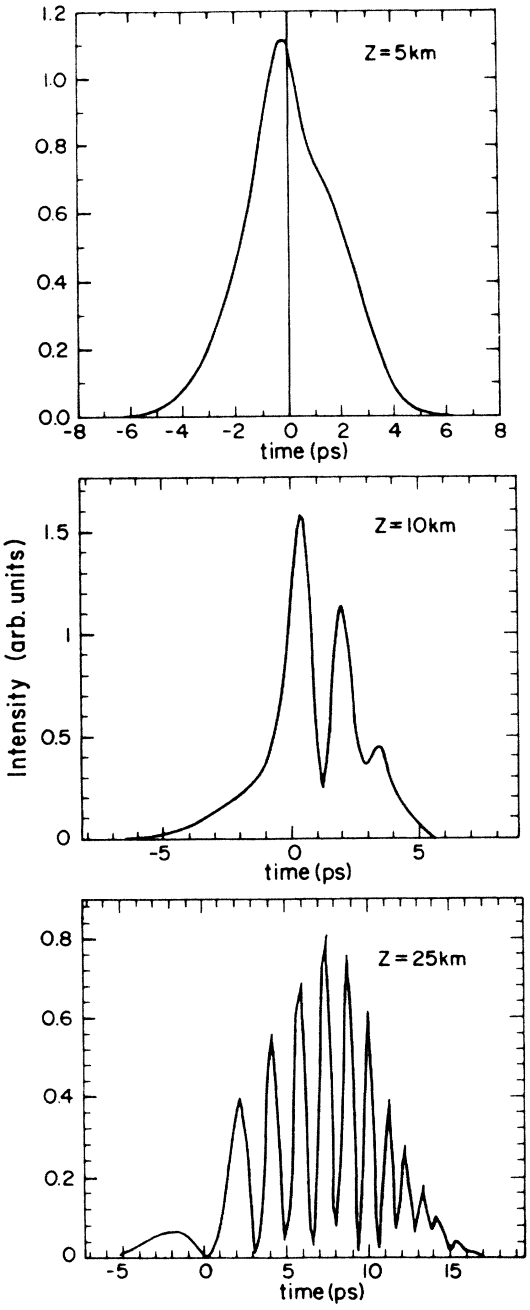

FIG. 8. Same parameters as in Fig. 6. Details of the pulse breakup are shown on an expanded scale at three distances during the initial stages of the pulse evolution.

assumes that they can be treated separately. More specifically, we assume that the effect of self-phase modulation occurring throughout the fiber length can be lumped at the input plane so that the effective field at $z>0$ that propagates in a purely dispersive medium is [see Eq. (3.1)]

$$A_{\text{eff}}(0,\tau)=A_0 f(\tau)\exp[i\phi_m \mid f^2(\tau)\mid], \tag{5.1}$$

where $f(\tau)$ is the initial shape and ϕ_m is given by Eq. (3.3). We leave $f(\tau)$ unspecified so that the following results are applicable to all pulse shapes. Propagation in a linear dispersive medium is accomplished using the general solution (4.1), and we obtain

$$A(z,\tau)=A_0 e^{-\gamma z}\int_{-\infty}^{\infty} g(\omega)\exp\left[i\omega\tau-\frac{i}{6}\beta^{(3)}\omega^3 z\right]d\omega\,, \tag{5.2}$$

where

$$g(\omega)=\frac{1}{2\pi}\int_{-\infty}^{\infty} f(\tau)\exp[i\phi_m \mid f^2(\tau)\mid]\exp(-i\omega\tau)d\tau \tag{5.3}$$

is the pulse spectrum that has been broadened due to nonlinearity-induced self-phase modulation.

The integral in Eq. (5.2) can be evaluated asymptotically using the method of stationary phase. The procedure is similar to that outlined in the Appendix for the case of a linear dispersive medium and the result is

$$A(z,\tau)=A_0 e^{-\gamma z}\left[\frac{\pi^2}{8\beta^{(3)}\tau z}\right]^{1/4} g\left[\left(\frac{2\tau}{\beta^{(3)}z}\right)^{1/2}\right]$$
$$\times\sin\left[\frac{2\tau}{3}\left(\frac{2\tau}{\beta^{(3)}z}\right)^{1/2}+\frac{\pi}{4}\right]. \tag{5.4}$$

In obtaining this asymptotic solution, we have assumed that $f(\tau)$ is an even function of τ. The pulse shape becomes asymmetric during propagation because of second-order dispersion. Equation (5.4) is valid only for $\tau>0$ and $z>z_c$, where z_c is defined by Eq. (4.6).

The asymptotic solution (5.4) can be used to study the qualitative features of the pulse shapes shown in Fig. 6 in the presence of both nonlinearity and dispersion. For the parameter values $\beta^{(3)}=0.2$ ps^3/km and $\tau_p=2.5$ ps, the asymptotic solution holds only for $z\gtrsim 40$ km [see Eq. (4.6)]. The presence of a sine function in Eq. (5.4) indicates the oscillatory structure or subpulses whose location is governed only by dispersion at a given distance (similar to the case of a linear medium). The amplitude of the subpulses is, however, determined by the spectral function $g(\omega)$ or by the nonlinearity [see Eq. (5.3)] since the spectrum is affected by the self-phase modulation (governed by ϕ_m). Equation (5.4) shows that all spectral features would manifest in the pulse shape with the mapping $\omega=(2\tau/\beta^{(3)}z)^{1/2}$. A separate evaluation of $g(\omega)$ using Eq. (5.3) shows that the observed envelope in Fig. 6 is indeed consistent with this interpretation. In particular, the double-peak superstructure is a direct consequence of the nonlinearity-induced spectral broadening of the pulse propagating inside the fiber. The superstructure remains unchanged (except for an overall scale factor) for $z=75$ and 100 km since, as discussed in Sec. III, the spectrum becomes frozen due to the saturation of ϕ_m in the presence of loss [see Eq. (3.3)]. We have verified that when $\gamma=0$ (no loss), the superstructure keeps evolving in response to the additional peaks generated in the pulse spectrum with an increase in ϕ_m.

VI. DISCUSSION AND CONCLUSION

In this paper we have considered the propagation of short optical pulses in dispersive, nonlinear fibers at the ZDWL, i.e., the wavelength at which group-velocity dispersion vanishes. It is found that the second-order dispersion in silica fibers is strong enough to cause significant pulse broadening and distortion. The relative importance of the nonlinear and dispersive effects depends on the initial pulse width τ_p. We have defined a characteristic time τ_c (typical value ~ 1 ps for dispersion-shifted silica fibers at 1.55 μm at a peak-power level ~ 10 mW) such that dispersion dominates for $\tau_p \ll \tau_c$ and nonlinearity dominates for $\tau_p \gg \tau_c$.

Using the parameters appropriate for a 1.55-μm dispersion-shifted single-mode fiber, we have studied the evolution of pulse shapes and pulse spectra along the fiber length for a wide range of initial pulse widths. For relatively short pulses such that $\tau_p \ll \tau_c$, the linear theory is approximately valid and the Airy-function solution[18] can describe well the qualitative features of the numerical results. For relatively broad pulses such that $\tau_p \gg \tau_c$, the pulse shape remains almost unchanged, except for the developing a slight asymmetry, since dispersion plays a minor role. The pulse spectrum, however, is considerably broadened due to the nonlinearity-induced self-phase modulation[26–29] and exhibits a multipeak structure that is slightly asymmetric because of second-order dispersion.

For pulse widths such that $\tau_p \sim \tau_c$, the mutual interaction between the dispersive and nonlinear effects introduces remarkably new features in the pulse shapes as well as the pulse spectra. Qualitatively speaking, the pulse is broadened and consists of a large number of subpulses whose width is governed mainly by the dispersion while their amplitude is governed mainly by the nonlinearity. The pulse exhibits a superstructure whose origin is related to the nonlinearity-induced self-phase modulation. The pulse spectrum is found to consist of two parts: a broad central structure related to nonlinearity and two narrow peaks of large amplitudes related to the periodic occurrence of dispersion-generated subpulses in the pulse shape (see Figs. 6 and 7). Further, in the presence of loss, after propagating a certain distance ($\simeq$50 km for a 0.2-dB/km loss) inside the fiber, the pulse acquires a spectrum that does not change with further propagation. These qualitative features in the pulse shape and spectrum are independent of the initial pulse shape.

An experimental observation of the above-mentioned theoretical predictions would be of considerable interest. Although the nonlinear pulse propagation in the presence of first-order fiber dispersion has been experimentally studied in relation to soliton formation,[2,31] the case of second-order dispersion at the ZDWL has attracted little attention. The main requirement for the experiment is a tunable picosecond laser source whose wavelength can be tuned to the ZDWL of the single-mode fiber. Either conventional fibers at 1.3 μm or dispersion-shifted fibers at 1.55 μm can be employed. A color-center laser can be useful[2] since it can be tuned in the vicinity of 1.55 μm. Alternatively, a mode-locked semiconductor laser[32] can be employed with temperature tuning used for a fine adjustment of the wavelength. We have estimated the tolerable wavelength detuning from the ZDWL so as to make the effect of first-order dispersion negligible, and find that for a pulse width $\tau_p \sim 1$ ps, the detuning should be less than 2 nm.

Our results suggest that significant pulse distortion occurring at the ZDWL can limit the performance of such fiberoptic communication systems. Equations (2.20) and (4.6) can be used to estimate the importance of pulse-distortion effects for given fiber parameters $\beta^{(3)}$ and $\bar{n}_2$. The peak power determines the characteristic time τ_c (pulse distortion occurs for $\tau_p \lesssim \tau_c$), while Eq. (4.6) provides the fiber length beyond which high-order dispersion limits the system performance. For peak powers $\gtrsim 10$ mW, the dispersive effects would limit the performance only at very high bit rates (> 100 GHz), although the exact matching of the carrier wavelength and the ZDWL would become more and more critical with an increase in the bit rate. At lower bit rates ($\lesssim 100$ GHz), Eq. (4.6) shows that the dispersive effects would manifest only for fiber lengths ~ 1000 km. For such ultralong communication systems (if possible in the future) the use of solitons may become an attractive option.[31]

APPENDIX: ASYMPTOTIC EVALUATION OF EQ. (4.1) USING THE METHOD OF STATIONARY PHASE

For an asymptotic evaluation of the integral appearing in Eq. (4.1), we rewrite it in the form

$$A(z,\tau)=e^{-\gamma z}\int_{-\infty}^{\infty}\tilde{A}(0,\omega)\exp[izf(\omega)]d\omega\ , \tag{A1}$$

where

$$f(\omega)=\frac{\tau}{z}\omega-\frac{1}{6}\beta^{(3)}\omega^3\ . \tag{A2}$$

In the method of stationary phase the integral (A1) is approximated by[33]

$$A(z,\tau)=e^{-\gamma z}\sum_j\left[\frac{i\pi}{2f''(\omega_j)z}\right]^{1/2}\times\tilde{A}(0,\omega_j)\exp[izf(\omega_j)]\ , \tag{A3}$$

where ω_j are the solutions of $df/d\omega=0$ and $f''(\omega_j)$ is the second derivative of $f(\omega)$ evaluated at ω_j. The method assumes that the most dominant contribution to the integral (A1) comes from the regions where $f(\omega)$ varies most slowly, i.e., the phase is stationary.

The frequencies ω_j corresponding to the extrema of $f(\omega)$ are obtained by using Eq. (A2) and setting $df/d\omega=0$. They are given by

$$\omega_j=\pm(2\tau/z\beta^{(3)})^{1/2}\ . \tag{A4}$$

For $\tau<0$, ω_j becomes imaginary and the method of steepest descent[33] should be used. However, for a discussion of the dispersion-induced oscillatory structure, the region $\tau>0$ is of interest (assuming $\beta^{(3)}>0$). A straightforward evaluation of Eq. (A3), using ω_j from Eq. (A4), gives the result

$$A(z,\tau)=e^{-\gamma z}\left[\frac{\pi^2}{8\beta^{(3)}\tau z}\right]^{1/4}\tilde{A}\left[0,\left[\frac{2\tau}{\beta^{(3)}z}\right]^{1/2}\right]$$
$$\times\sin\left[\frac{2\tau}{3}\left[\frac{2\tau}{\beta^{(3)}z}\right]^{1/2}+\frac{\pi}{4}\right], \quad \text{(A5)}$$

where

$$\tilde{A}(0,\omega)=\frac{1}{2\pi}\int_{-\infty}^{\infty}A(0,\tau)\exp(-i\omega\tau)d\tau\ . \quad \text{(A6)}$$

In obtaining Eq. (A5), we have assumed that $A(0,\tau)$ is an even function of τ, i.e., the pulse is initially symmetric at the input plane $z=0$. During propagation, the pulse becomes asymmetric because of second-order dispersion. Equation (A5) is valid for $\tau>0$ and large z satisfying Eq. (4.6).

For an initially Gaussian pulse, Eq. (A5) is identical to that obtained using Eq. (4.3) with the asymptotic expansion (4.7). Equation (A5) is, however, valid for arbitrary pulse shapes. The important point to note is that the subpulse structure is governed by the sinusoidal function and is independent of the pulse shape. In particular, the pulse intensity becomes zero whenever the argument of the sine function is an integer multiple of 2π, and for the mth zero, τ_m is given by Eq. (4.10). The amplitude of the subpulses is governed by the pulse shape. Equation (A5) shows that the generation of subpulses in the dispersive medium at the ZDWL is a general phenomenon, independent of the shape and the width of the launched pulse.

[1]A. Hasegawa and F. Tappert, Appl. Phys. Lett. **23**, 142 (1973); A. Hasegawa and Y. Kodama, Proc. IEEE **69**, 1145 (1981).

[2]L. F. Mollenauer R. H. Stolen, and J. P. Gordon, Phys. Rev. Lett. **45**, 1095 (1980).

[3]N. J. Doran and K. J. Blow, IEEE J. Quantum Electron. **QE-19**, 1883 (1983); K. J. Blow and N. J. Doran, Electron. Lett. **19**, 429 (1983).

[4]D. Anderson, Phys. Rev. A **27**, 3135 (1983); D. Anderson and M. Lisak, *ibid.* **27**, 1393 (1983).

[5]K. J. Blow, N. J. Doran, and E. Cummins, Opt. Commun. **48**, 181 (1983).

[6]V. A. Vysloukh, Kvant. Elektron. **10**, 1668 (1983) [Sov. J. Quantum Electron. **13**, 1113 (1983)].

[7]I. N. Sisakyan and A. B. Shvartsburg, Kvant. Elektron. **11**, 1703 (1984) [Sov. J. Quantum Electron. **14**, 1146 (1984)].

[8]H. E. Lassen, F. Mengel, B. Tromberg, N. Albertsen, and P. L. Christiansen, Opt. Lett. **10**, 34 (1985).

[9]M. J. Potasek, G. P. Agrawal, and S. C. Pinault, J. Opt. Soc. Am. B (to be published).

[10]V. E. Zakharov and A. B. Shabat, Zh. Eksp. Teor. Fiz. **61**, 118 (1971) [Sov. Phys.—JETP **34**, 62 (1972)].

[11]J. Satsuma and N. Yajima, Prog. Theor. Phys. Suppl. **55**, 284 (1974).

[12]A. Sugimura, K. Daikoku, N. Imoto, T. Miya, IEEE J. Quantum Electron. **QE-16**, 215 (1980).

[13]P. D. Lazay and A. D. Pearson, IEEE J. Quantum Electron. **QE-18**, 504 (1982).

[14]U. C. Paek, G. E. Peterson, and A. Carnevale, Bell. Syst. Tech. J. **60**, 583 (1981).

[15]M. A. Saifi, S. J. Jang, L. G. Cohen, and J. Stone, Opt. Lett. **7**, 43 (1982).

[16]S.-J. Jang, J. Sanchez, K. D. Pohl, and L. D. Lésperance, J. Lightwave Tech. **LT-2**, 313 (1984).

[17]H.-T. Shang, T. A. Lenahan, P. F. Glodis, and D. Kalish, Electron. Lett. **21**, 201 (1985).

[18]M. Miyagi and S. Nishida, Appl. Opt. **18**, 678 (1979).

[19]D. Marcuse, Appl. Opt. **19**, 1653 (1980).

[20]E. A. Sziklas and A. E. Siegman, Appl. Opt. **14**, 1874 (1975).

[21]M. D. Feit and J. A. Fleck, Appl. Opt. **17**, 3990 (1978).

[22]J. Van Roey, J. van der Donk, and P. E. Lagasse, J. Opt. Soc. Am. **71**, 803 (1981).

[23]M. Lax, J. H. Batteh, and G. P. Agrawal, J. Appl. Phys. **52**, 109 (1981).

[24]G. P. Agrawal, J. Appl. Phys. **56**, 3100 (1984).

[25]J. W. Cooley and J. W. Tukey, Math. Comput. **19**, 297 (1965).

[26]R. H. Stolen and C. Lin, Phys. Rev. A **17**, 1448 (1978).

[27]F. Shimizu, Phys. Rev. Lett. **19**, 1097 (1967).

[28]T. K. Gustafson, J. P. E. Taran, H. A. Haus, J. R. Lifsitz, and P. L. Kelley, Phys. Rev. **177**, 306 (1969).

[29]E. P. Ippen, C. V. Shank, and T. K. Gustafson, Appl. Phys. Lett. **24**, 190 (1974).

[30]*Handbook of Mathematical Functions,* edited by M. Abramowitz and I. A. Stegun (Dover, New York, 1970), p. 448.

[31]L. F. Mollenauer, R. H. Stolen, and M. N. Islam, Opt. Lett. **10**, 229 (1985).

[32]G. Eisenstein, R. S. Tucker, S. K. Korotky, U. Koren, J. J. Veselka, L. W. Stulz, R. M. Jopson, and K. L. Hall, Electron. Lett. **21**, 173 (1985).

[33]H. Jeffreys and B. S. Jeffreys, *Methods of Mathematical Physics* (Cambridge University Press, London, 1978), Chap. 17.